Eur. Phys. J. A **25**, 365–378 (2005)
DOI 10.1140/epja/i2005-10130-3

THE EUROPEAN PHYSICAL JOURNAL A

Origin of three-body resonances

E. Garrido[1,a], D.V. Fedorov[2], and A.S. Jensen[2]

[1] Instituto de Estructura de la Materia, CSIC, Serrano 123, E-28006 Madrid, Spain
[2] Department of Physics and Astronomy, University of Aarhus, DK-8000 Aarhus C, Denmark

Received: 16 April 2005 / Revised version: 7 July 2005 /
Published online: 13 October 2005 –
Communicated by G. Orlandini

Abstract. We expose the relation between the properties of the three-body continuum states and their two-body subsystems. These properties refer to their bound and virtual states and resonances, all defined as poles of the S-matrix. For one infinitely heavy core and two non-interacting light particles, the complex energies of the three-body poles are the sum of the two two-body complex pole-energies. These generic relations are modified by center-of-mass effects which alone can produce a Borromean system. We show how the three-body states evolve in ^{6}He, ^{6}Li, and ^{6}Be when the nucleon-nucleon interaction is continuously switched on. The schematic model is able to reproduce the main properties in their spectra. Realistic calculations for these nuclei are shown in detail for comparison. The implications of a core with non-zero spin are investigated and illustrated for ^{17}Ne ($^{15}\mathrm{O}+p+p$). Dimensionless units allow predictions for systems of different scales.

PACS. 21.45.+v Few-body systems – 31.15.Ja Hyperspherical methods – 25.70.Ef Resonances – 11.80.Jy Many-body scattering and Faddeev equation

1 Introduction

The three-body problem has a long history from macroscopic celestial classical mechanics, *e.g.* Sun-Earth-Moon [1] to microscopic quantum mechanics, *e.g.* the helium atom [2], three nucleons [3] or three quarks [4]. The modern treatment was boosted by the formulation of the Faddeev equations [5] originally aimed at scattering problems, but also successfully applied for bound states [6, 7]. The more recent interest in bound-state halo structures and Borromean systems are by now fairly well understood in terms of the basic two-body interactions [8]. The success is at least indisputable for three-body systems with only one or a few bound states.

On the other hand, the corresponding three-body properties for positive energies (energies above breakup) are much less established although studied thoroughly for both short- and long-range interactions [2, 9]. Contributions from both short- and long-range interactions make computations numerically difficult. The three-body Coulomb problem itself is still considered unsolved [10–12] and three-body resonances for strongly interacting particles are still debated [13–17]. This is unfortunate, since the continuum structure often forms the basis in descriptions of the dynamic behavior of a given system.

Crucial properties of the continuum are revealed by information about the resonances and virtual states defined as poles of the S-matrix. Together with the discrete set of bound negative-energy states we also have a discrete set of unbound complex-energy states with their corresponding wave functions. For completeness also the continuous non-singular background states are needed, but the singularities of the scattering matrix are very often decisive. Important examples using different methods within few-body physics are astrophysical reaction rates [18], adiabatic reaction processes arising at low energies or for large impact parameters [19], three-body decays [20], three-body resonances for Faddeev operators [21], for nucleons [22], for electrons and positrons [23] and four-body nuclear continuum states [24]. This list could be extended.

Continuum structure is in general more difficult than bound-state problems although various methods have been designed to overcome the technical problems at least for resonances, see for example [9, 15–17, 25, 26]. An understanding of the generic origin of S-matrix poles would be tremendously helpful especially if recognizable traces of a well-structured origin are left in the realistic spectra. No doubt this would allow easier interpretation of complicated numerical results, allowed design of better methods, and indicate which effects to look for in different contexts.

The purpose of this work is to investigate how the two-body interactions determine the three-body continuum

[a] e-mail: e.garrido@iem.cfmac.csic.es

structure. We focus on three-body continuum states where none of the two-body subsystems is bound (Borromean systems). When two-body bound states are possible, different three-body structures can appear, as for instance, unbound three-body states with negative energy. However, these systems can very often be understood as two-body systems made by a two-body bound state and the remaining third particle in the continuum. With the help of the hyperspheric adiabatic expansion method we determine what three-body bound or virtual states and resonances result from given sets of corresponding two-body properties. Taking a simple system as starting point, it is then possible to observe how the three-body states evolve in the complex energy plane when more and more realistic features are incorporated into the calculation.

In sect. 2 we give details about the complex scaled adiabatic expansion methods. In sect. 3 the schematic system of an infinitely heavy core and two mutually non-interacting light particles is described analytically, while in sect. 4 the general properties of the system are described after numerical studies of specific systems. In sect. 5 we relate the spectra from the schematic model with those obtained in realistic calculations for systems with zero (^{6}He, ^{6}Li, ^{6}Be) and non-zero core-spin (^{17}Ne). We finish in sect. 6 with some qualitative estimates for other systems and in sect. 7 we give a short summary and the conclusions.

2 The complex scaled hyperspheric adiabatic expansion method

To describe a three-body system we use the standard coordinates:

$$\begin{aligned} \boldsymbol{x}_i &= \sqrt{\frac{m_j m_k}{m(m_j+m_k)}}(\boldsymbol{r}_j - \boldsymbol{r}_k)\ , \\ \boldsymbol{y}_i &= \sqrt{\frac{m_i(m_j+m_k)}{m(m_i+m_j+m_k)}}\left(\boldsymbol{r}_i - \frac{m_j\boldsymbol{r}_j + m_k\boldsymbol{r}_k}{m_j+m_k}\right), \end{aligned} \tag{1}$$

where m_i, m_j, and m_k are the masses of the three particles and m is an arbitrary normalization mass. From the Jacobi coordinates we define the hyperspheric coordinates $\{\rho, \Omega_i\}$, where $\{\Omega_i\} = \{\alpha_i, \Omega_{x_i}, \Omega_{y_i}\}$, $\rho = \sqrt{x_i^2 + y_i^2}$, $\alpha_i = \arctan(x_i/y_i)$, and Ω_{x_i} and Ω_{y_i} give the directions of $\boldsymbol{x}_i$ and $\boldsymbol{y}_i$, respectively.

The three-body wave function is written as a sum of three components $\psi^{(i)}(\boldsymbol{x}_i, \boldsymbol{y}_i)$, each corresponding to one of the three possible sets of Jacobi coordinates [7]. These three components satisfy the three Faddeev equations

$$\begin{aligned} &(T-E)\psi^{(i)}(\boldsymbol{x}_i,\boldsymbol{y}_i) + V_{jk}(x_i) \\ &\times\left(\psi^{(i)}(\boldsymbol{x}_i,\boldsymbol{y}_i) + \psi^{(j)}(\boldsymbol{x}_j,\boldsymbol{y}_j) + \psi^{(k)}(\boldsymbol{x}_k,\boldsymbol{y}_k)\right) = 0, \end{aligned} \tag{2}$$

where T is the kinetic energy operator, $V_{jk}(x_i)$ is the two-body interaction between particles j and k, and E is the three-body energy. Here (i,j,k) is a cyclic permutation of $(1,2,3)$.

We employ the hyperspheric coordinates to expand each component $\psi^{(i)}(\boldsymbol{x}_i, \boldsymbol{y}_i)$ in terms of a complete set of angular functions $\phi_n^{(i)}$,

$$\psi_{n_0}^{(i)}(\boldsymbol{x}_i,\boldsymbol{y}_i) = \frac{1}{\rho^{5/2}}\sum_n f_n^{(n_0)}(\rho)\phi_n^{(i)}(\rho,\Omega_i), \tag{3}$$

where the additional index n_0 labels different solutions we later on want to consider. Usually the expansion (3) converges rather fast, and only a few terms (typically no more than three) are needed.

By rewriting eq. (2) in terms of the hyperspheric coordinates, and inserting the expansions in eq. (3) we separate the Faddeev equations into angular and radial parts:

$$(\hat{\Lambda}^2 - \lambda_n(\rho))\phi_n^{(i)} - \frac{2m\rho^2}{\hbar^2}V_{jk}^{(i)}(x_i)\left(\phi_n^{(i)} + \phi_n^{(j)} + \phi_n^{(k)}\right) = 0\ , \tag{4}$$

$$\left[-\frac{\mathrm{d}^2}{\mathrm{d}\rho^2} - \frac{2mE}{\hbar^2} + \frac{1}{\rho^2}\left(\lambda_n(\rho) + \frac{15}{4}\right)\right] f_n^{(n_0)}(\rho) = \sum_{n'}\left(2P_{nn'}\frac{\mathrm{d}}{\mathrm{d}\rho} + Q_{nn'}\right) f_{n'}^{(n_0)}(\rho)\ , \tag{5}$$

where $\hat{\Lambda}^2$ is a hyperangular operator which together with expressions for the functions $P_{nn'}(\rho)$ and $Q_{nn'}(\rho)$ can be found in [7]. The complete set of angular functions $\phi_n^{(i)}$ in the expansion (3) are precisely the eigenfunctions of the angular part of the Faddeev equations. The index n labels the corresponding eigenvalue λ_n, which enters in the coupled set of radial equations (5) as effective potentials. The index n_0 is related to the boundary condition for continuum wave functions, which for short-range interactions and no two-body bound states has the asymptotics given by [7]

$$f_n^{(n_0)}(\kappa\rho) \longrightarrow \sqrt{\kappa\rho}\left[H_{K+2}^{(2)}(\kappa\rho)\delta_n^{n_0} + S_n^{n_0}(\kappa)H_{K+2}^{(1)}(\kappa\rho)\right], \tag{6}$$

where n_0 then labels the incoming channel, the S-matrix $S_n^{n_0}$ is a factor depending on the complex momentum κ related to the complex energy E by $\kappa = \sqrt{2mE/\hbar^2}$, and $H_K^{(1)}$ and $H_K^{(2)}$ are Hankel functions of first and second kind. The hypermomentum K is given by the asymptotic behaviour of the angular eigenvalue $\lambda_n(\rho)$ that approaches $K(K+4)$ [7].

For three-body bound states $f_n^{(n_0)}$ must fall off exponentially at large distances. Then only one Hankel function is present and the S-matrix $S_n^{n_0}$ has a pole for the imaginary momentum κ ($\kappa = i|\kappa|$) and the energy E is negative. Poles of the S-matrix in the lower half of the complex momentum plane correspond to three-body resonances, and their asymptotic radial wave function is given only by the $H_{K+2}^{(1)}$ part in eq. (6). Asymptotically the Hankel function $H_{K+2}^{(2)}$ vanishes exponentially like $e^{-|\kappa|\rho}$, while $H_{K+2}^{(1)}$ grows like $e^{|\kappa|\rho}$. This means that the radial coefficients of the continuum wave functions are dominated by the $H_{K+2}^{(1)}$ part. Therefore, it is very difficult to distinguish the resonance wave function, where

only the $H^{(1)}_{K+2}$ term is present in the asymptotics, from an ordinary continuum wave function.

This problem is solved by applying the complex scaling method [25, 27–30], where the Jacobi coordinates x_i and y_i are rotated into the complex plane by an arbitrary angle θ ($x_i \to x_i e^{i\theta}$, $y_i \to y_i e^{i\theta}$). This means that only the hyperradius ρ is rotated ($\rho \to \rho e^{i\theta}$), while the five hyperangles $\{\Omega_i\}$ remain unchanged. After this rotation the radial wave functions of the resonances behave asymptotically like

$$f^{(n_0)}_n(\kappa\rho e^{i\theta}) \to \sqrt{\rho} H^{(1)}_{K+2}(|\kappa|\rho e^{i(\theta-\theta_R)}) \to e^{-|\kappa|\rho\sin(\theta-\theta_R)} e^{i(|\kappa|\rho\cos(\theta-\theta_R)-K\pi/2+3\pi/4)}, \quad (7)$$

where θ_R is the argument of the complex momentum κ ($\kappa = |\kappa|e^{-i\theta_R}$). From (7) we observe that when $\theta > \theta_R$ the radial wave function falls off exponentially, exactly as a bound state. Continuum wave functions are dominated in the asymptotics by the $H^{(2)}_{K+2}(|\kappa|\rho e^{i(\theta-\theta_R)})$ term, that diverges exponentially when $\theta > \theta_R$. Thus, after complex scaling, resonances can be easily distinguished from ordinary continuum states, and furthermore, the numerical technique used to compute bound states can be used for resonances. In particular, after solving the complex scaled equations (4) and (5) with the boundary condition (7) three-body resonances and bound states are simultaneously obtained. Solving eq. (5) with a box boundary condition ($f(\rho_{max}) = 0$, ρ_{max} being a large value of the hyperradius) discretizes the continuum spectrum, and the continuum states are rotated by an angle θ in the momentum plane and 2θ in the energy plane [25]. The box boundary condition is often enough to obtain accurate bound state and resonance solutions.

3 Two independent subsystems

We analyze in this section the schematic model of an infinitely heavy core and two light particles. These two mutually non-interacting light particles interact with the core via short-range interactions. We shall first assume that these three particles have zero spin and then later generalize to non-zero particle spins.

3.1 Particles without spin

From the Jacobi coordinates (1) we can construct the corresponding conjugated momenta:

$$\boldsymbol{k}_{x_i} = \sqrt{\frac{m m_j m_k}{m_j + m_k}} \left(\frac{\boldsymbol{p}_j}{m_j} - \frac{\boldsymbol{p}_k}{m_k} \right), \quad \boldsymbol{k}_{y_i} = \sqrt{\frac{m m_i (m_j + m_k)}{(m_i + m_j + m_k)}} \left(\frac{\boldsymbol{p}_i}{m_i} - \frac{\boldsymbol{p}_j + \boldsymbol{p}_k}{m_j + m_k} \right). \quad (8)$$

In precise analogy to the hyperradial coordinates, we now introduce the hypermomentum coordinates $\{\kappa, \Omega_{\kappa_i}\}$ defined as $\{\Omega_{\kappa_i}\} = \{\alpha_{\kappa_i}, \Omega_{k_{x_i}}, \Omega_{k_{y_i}}\}$, $\kappa = \sqrt{k^2_{x_i} + k^2_{y_i}}$, $\alpha_{\kappa_i} = \arctan(k_{x_i}/k_{y_i})$. The three-body momentum κ defined earlier is independent of the Jacobi coordinate system labeled i. The directions of $\boldsymbol{k}_{x_i}$ and $\boldsymbol{k}_{y_i}$ are described by $\Omega_{k_{x_i}}$ and $\Omega_{k_{y_i}}$, respectively.

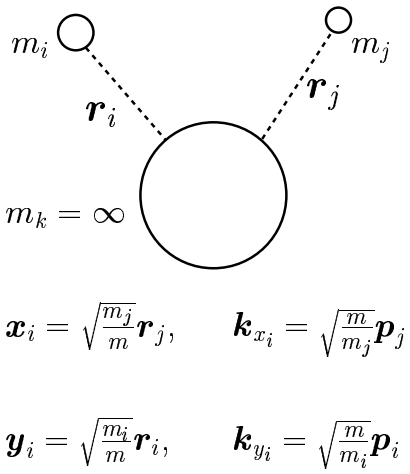

Fig. 1. Sketch of the schematic three-body system. Particles i and j do not interact with each other. Particle k is infinitely heavy. One set of Jacobi coordinates and their corresponding conjugate momenta are given in the lower part.

When one of the three spinless particles has infinite mass (let us take $m_k = \infty$), eqs. (1) and (8) simplify, in the three-body center-of-mass system where $\boldsymbol{r}_k = 0$ and $\boldsymbol{p}_i + \boldsymbol{p}_j + \boldsymbol{p}_k = 0$, to the form in fig. 1. Therefore, in two of the three possible sets of Jacobi coordinates, the coordinates are simply proportional to the distances between the infinitely heavy core and each of the two light particles. If the two-body interactions depend only on the distance between particles, the three-body Hamiltonian H can be written as $H = H_{ki} + H_{kj}$ (see fig. 1) where H_{ki} and H_{kj} are the two-body Hamiltonians describing the corresponding two-body systems. From this separability, the three-body bound-state energies are obviously given by the sum of the corresponding two-body bound-state energies.

For three-body resonances and virtual states the same happens. Three-body resonances show up at energies equal to the sum of the two-body resonance energies of the ki and kj subsystems. From the separability of the Hamiltonian this result may be accepted as obvious. However, the only trivial deduction using the separability is that the three-body energy is given by the sum of the two two-body energies. This does not necessarily imply that a three-body energy equal to the sum of two two-body resonance energies must correspond to a three-body resonance. Bound states have discrete energies, and the split of a given three-body bound-state energy into two two-body energies can be made only in specific ways, since the two-body energies can have only the specific values corresponding to the discrete two-body bound-state spectrum. However, resonances are continuum states, and then a given three-body energy can be obtained by infinitely many pairs of two-body energies. Therefore, if a given three-body energy matches with the sum of two two-body resonance energies, there are also infinitely many other pairs of

continuum (non-resonant) two-body energies whose sum gives the same three-body energy. Thus, it is not a trivial conclusion that only the particular three-body state of matching energy corresponds to a three-body resonance defined as a pole in the three-body S-matrix.

Let us then investigate this more closely. From the separability of the Hamiltonian it follows that the three-body wave function is the product of the wave functions describing the ki and kj two-body subsystems. For unbound two-body systems the two-body wave function can be expanded in partial waves, and the three-body wave function takes then the form

$$\Psi^{(+)}(\boldsymbol{x},\boldsymbol{y},\boldsymbol{k}_x,\boldsymbol{k}_y) = \left(\sqrt{\frac{2}{\pi}}\sum_{\ell_x m_{\ell_x}} i^{\ell_x}\frac{u_{\ell_x}(x,k_x)}{xk_x}Y_{\ell_x m_{\ell_x}}(\Omega_x)Y^{\star}_{\ell_x m_{\ell_x}}(\Omega_{k_x})\right) \times\left(\sqrt{\frac{2}{\pi}}\sum_{\ell_y m_{\ell_y}} i^{\ell_y}\frac{u_{\ell_y}(y,k_y)}{yk_y}Y_{\ell_y m_{\ell_y}}(\Omega_y)Y^{\star}_{\ell_y m_{\ell_y}}(\Omega_{k_y})\right), \tag{9}$$

where $(\boldsymbol{x},\boldsymbol{y})$ refer to the Jacobi system in fig. 1 and the momenta of the corresponding subsystems are $\boldsymbol{k}_x$ and $\boldsymbol{k}_y$. The spherical harmonics and the two-body radial functions are denoted $Y_{\ell m_\ell}$ and u_ℓ.

Following [19], also the continuum wave function for a three-body system of spinless particles can be written as

$$\Psi^{(+)}(\boldsymbol{x},\boldsymbol{y},\boldsymbol{k}_x,\boldsymbol{k}_y) = \sum_{KLM\ell_x\ell_y} Y^{(\ell_x\ell_y)*}_{KLM}(\Omega_\kappa) \times\sum_{K'L'M'\ell'_x\ell'_y} f^{(K'\ell'_x\ell'_yL')}_{K\ell_x\ell_yL}(\kappa\rho)Y^{(\ell'_x\ell'_y)}_{K'L'M'}(\Omega) \tag{10}$$

where $(\boldsymbol{x},\boldsymbol{y})$, $(\boldsymbol{k}_x,\boldsymbol{k}_y)$, Ω and Ω_κ could correspond to any of the three possible sets of Jacobi systems. We omitted the index i. The hyperradial functions, $f^{(K'\ell'_x\ell'_yL')}_{K\ell_x\ell_yL}$, are solutions to eq. (5) where we now specified the indices n and n_0 and explicitly included the factor κ in the argument. The hyperspheric harmonics $Y^{(\ell_x\ell_y)}_{KLM}(\Omega)$ can for instance be found in [7]. Using the orthogonality of the hyperspheric harmonics, we immediately have

$$f^{(K'\ell'_x\ell'_yL')}_{K\ell_x\ell_yL}(\kappa\rho) = \int \mathrm{d}\Omega\int \mathrm{d}\Omega_\kappa \Psi^{(+)}(\boldsymbol{x},\boldsymbol{y},\boldsymbol{k}_x,\boldsymbol{k}_y) \times Y^{(\ell_x\ell_y)}_{KLM}(\Omega_\kappa)Y^{(\ell'_x\ell'_y)*}_{K'L'M'}(\Omega) \tag{11}$$

and by inserting eq. (9) into (11) we get

$$f^{(K'\ell'_x\ell'_yL')}_{K\ell_x\ell_yL}(\kappa\rho) = \delta_{\ell_x\ell'_x}\delta_{\ell_y\ell'_y}\delta_{LL'}\frac{2}{\pi}i^{\ell_x+\ell_y}N^{\ell_x\ell_y}_K N^{\ell_x\ell_y}_{K'} \times\int_0^{\pi/2}\mathrm{d}\alpha_\kappa(\sin\alpha_\kappa)^{\ell_x+2}(\cos\alpha_\kappa)^{\ell_y+2}P^{(\ell_x+\frac{1}{2},\ell_y+\frac{1}{2})}_n(\cos 2\alpha_\kappa) \times\int_0^{\pi/2}\mathrm{d}\alpha(\sin\alpha)^{\ell_x+2}(\cos\alpha)^{\ell_y+2}P^{(\ell_x+\frac{1}{2},\ell_y+\frac{1}{2})}_{n'}(\cos 2\alpha) \times\frac{u_{\ell_x}(x,k_x)}{xk_x}\frac{u_{\ell_y}(y,k_y)}{yk_y}, \tag{12}$$

where $N^{\ell_x\ell_y}_K$ is the normalization constant appearing when expressing the hyperspheric harmonics in terms of the spherical harmonics and the Jacobi polynomials [7]. Due to the delta functions, the three-body hyperradial functions in eq. (12) are block-wise diagonal and each block matrix can, for given (ℓ_x,ℓ_y,L), be labeled by the indexes KK'. Note also that the wave function does not depend on the total orbital angular momentum L. All L-values allowed by coupling are degenerate.

In the limit of zero interactions between the core and the light particles the two-body radial wave functions $u_\ell(x,k)/xk$ become the spherical Bessel function $j_\ell(xk)$, and eq. (12) becomes

$$f^{(K'\ell'_x\ell'_yL')}_{K\ell_x\ell_yL}(\kappa\rho) = \delta_{\ell_x\ell'_x}\delta_{\ell_y\ell'_y}\delta_{LL'}\delta_{KK'}i^K\frac{J_{K+2}(\kappa\rho)}{(\kappa\rho)^2}, \tag{13}$$

where J_{K+2} is a Bessel function of the first kind. Inserting (13) into (10) we then obtain the three-body wave function

$$\Psi^{(+)}(\boldsymbol{x},\boldsymbol{y},\boldsymbol{k}_x,\boldsymbol{k}_y) = \sum_{K\ell_x\ell_yLM} i^K\frac{J_{K+2}(\kappa\rho)}{(\kappa\rho)^2}Y^{(\ell_x\ell_y)*}_{KLM}(\Omega_\kappa)Y^{\ell_x\ell_y}_{KLM}(\Omega) \equiv \frac{1}{(2\pi)^3}e^{i(\boldsymbol{k}_x\cdot\boldsymbol{x}+\boldsymbol{k}_y\cdot\boldsymbol{y})} \tag{14}$$

and the plane waves are recovered from the hyperradial partial wave expansion.

The large-distance asymptotic behaviour of the three-body radial wave functions, eq. (12), can be obtained from the asymptotics of the two-body wave functions, that for the case in which none of the two-body core-particle subsystems is bound has the form

$$\frac{u_\ell(x,k)}{xk} \to \frac{1}{2}\left(h^{(2)}_\ell(xk) + s_\ell(k)h^{(1)}_\ell(xk)\right), \tag{15}$$

where $h^{(i)}_\ell$ are the corresponding two-body Hankel functions of first and second kind, and $s_\ell(k)$ is the two-body S-matrix. Inserting eq. (15) into (12) and using the expressions given in the appendix, we obtain

$$f^{(K')}_K(\kappa\rho) \longrightarrow \frac{i^{K'}}{(\kappa\rho)^2}\left[H^{(2)}_{K+2}(\kappa\rho)\delta^{K'}_K + S^{K'}_K(\kappa)H^{(1)}_{K+2}(\kappa\rho)\right], \tag{16}$$

where we omitted the unimportant block indexes (ℓ_x,ℓ_y,L). Then eq. (16) is identical to eq. (6) after division by the phase factor $1/\rho^{5/2}$ in eq. (3). The three-body S-matrix takes the form

$$S^{K'}_K(\kappa) = \frac{2\int_0^{\pi/2}\mathrm{d}\alpha_\kappa\Phi^{(\ell_x\ell_y)}_{nn'}(\alpha_\kappa)s_{\ell_x}(k_x)s_{\ell_y}(k_y)}{\int_0^{\pi/2}\mathrm{d}\alpha_\kappa\Phi^{(\ell_x\ell_y)}_{nn'}(\alpha_\kappa)(s_{\ell_x}(k_x)+s_{\ell_y}(k_y))}, \tag{17}$$

where

$$\Phi^{(\ell_x\ell_y)}_{nn'}(\alpha_\kappa) = (\sin\alpha_\kappa)^{2\ell_x+2}(\cos\alpha_\kappa)^{2\ell_y+2} \times P^{(\ell_x+\frac{1}{2},\ell_y+\frac{1}{2})}_n(\cos 2\alpha_\kappa)P^{(\ell_x+\frac{1}{2},\ell_y+\frac{1}{2})}_{n'}(\cos 2\alpha_\kappa), \tag{18}$$

is a smooth function of α_κ given in terms of the Jacobi functions $P_n^{(\ell_x+\frac{1}{2},\ell_y+\frac{1}{2})}$ with $K = 2n + \ell_x + \ell_y$ and $K' = 2n' + \ell_x + \ell_y$.

The integrands in eq. (17) contain the two-body S-matrices depending on corresponding momenta. The integration variable maintains the total energy of the two subsystems while varying the ratio of their momenta. Assume that one pole of one of the subsystems is a first-order pole which does not coincide with any pole of the other subsystem, then the integrations in eq. (17) across the pole give a smooth function without trace of the pole. However, if two poles from different subsystems exist simultaneously the product of two-body S-matrices in the numerator of eq. (17) results in a pole term of second order, which after integration across the pole, leaves a first-order pole in the three-body S-matrix. The energy of this three-body pole corresponds then precisely to the sum of the energies of the two two-body poles.

If one pole is of higher order, and not coinciding with a pole from the other subsystem, it would survive the integration precisely in the same way in numerator and denominator. Thus no trace is left in the three-body S-matrix. A three-body pole only arises when two two-body poles belonging to different subsystems exist simultaneously. Combining any order of coinciding poles from the two subsystems is then seen to produce a three-body pole of an order equal to the smallest order of the two-body poles involved. This proves that the three-body poles appear if and only if the energy is equal to the sum of energies of two two-body poles from different subsystems. The smallest order of the two coinciding poles reappears in the three-body pole.

In case of having a two-body bound state, the corresponding two-body asymptotics is not given by eq. (15) but by a falling off exponential e^{-kx}, where k is determined by the two-body binding energy. The three-body properties are then directly dictated by the two-body S-matrix describing the remaining core-particle subsystem. If this two-body S-matrix has a pole corresponding to a two-body bound state, the three-body system is obviously bound with a binding energy equal to the sum of the two two-body binding energies. If the two-body S-matrix has a pole corresponding to a two-body resonance (or virtual state), the three-body system has then a resonance (or virtual state) that actually corresponds to a resonance (or virtual state) of the two-body system made by the bound two-body state and the remaining third particle.

At this point it is also important to mention that we are identifying poles of the S-matrix in the fourth quadrant of the energy plane and resonances. However, strictly speaking, for a pole to be considered a resonance it is required that its width is clearly smaller than the energy separation between resonances. In this way resonances are the poles of the S-matrix close enough to the real energy axis. It can certainly happen that when two complex energies corresponding to two singularities in the S-matrix are added, the final energy can be close to the negative imaginary axis, or even in the third quadrant of the energy plane. These singularities should not be considered as resonances in the sense given above.

The formalism leading to the expression for the three-body S-matrix is applicable for a very different system, *i.e.* three particles of finite mass with only one non-vanishing two-body interaction. If we choose the Jacobi coordinate system where $\boldsymbol{x}$ is related to the non-zero two-body interaction the wave function is again given by eq. (9) with a Bessel function instead of $u_{\ell_y}/(yk_y)$. All derivations remain unchanged and we arrive at the S-matrix in eq. (17). The difference is that now only the two-body S-matrix related to the $\boldsymbol{x}$-degree of freedom has poles. Therefore the three-body system has no S-matrix poles.

This system effectively also consists of two independent two-body systems, but now reached in a completely different limit with one non-zero interaction and arbitrary masses. The result then illustrates other aspects of the continuum properties for three-body systems. In both cases the conclusion is that one subsystem alone cannot produce three-body resonances or virtual states. At least two different subsystems must collaborate and simultaneously contribute with coinciding poles. It then seems inevitable that, if all the three two-body subsystems only have poles, then fully realistic three-body systems must also have only poles.

3.2 Particles with spin

The results in the previous subsection remain valid for particles of non-zero spin if the two-body interactions are spin-independent, because then the spin part of the wave function is decoupled from the coordinate part. In fact, even in the case of identical particles the spin part can always be used to establish the proper (anti)symmetry of the wave function without changing the coordinate part. The only exception is two identical bosons with zero spin where the spin part of the wave function always is symmetric under exchange of the two bosons. Therefore odd values of the relative orbital angular momentum between the bosons are strictly forbidden. This fact leads to important differences compared to non-identical particles [31].

When the two-body interactions are spin dependent, the separability of the three-body Hamiltonian for the system shown in fig. 1 can disappear. We denote the spins of particles i, j, and k by s_i, s_j, and s_k, respectively. Let us for simplicity assume that the particle-core interactions of the system in fig. 1 contain a central plus a spin-spin term, *i.e.*, $V_{ki} = V_c^{(ki)} + V_{ss}^{(ki)} \boldsymbol{j}_i \cdot \boldsymbol{s}_k$, where $\boldsymbol{j}_i = \boldsymbol{\ell}_{ki} + \boldsymbol{s}_i$ and $\boldsymbol{\ell}_{ki}$ is the relative orbital angular momentum between the core and particle i (and similarly for the V_{kj} interaction). As shown in [26], this type of spin-spin operator is especially convenient, since it guarantees conservation of the quantum number j_i in agreement with the intrinsic motion of particles in the core possibly being identical to the particles of the three-body system.

The two-body Hamiltonian H_{ki} is then diagonal in the basis $\{|s_k, (s_i, \ell_{ki})j_i; j_{ki}\rangle\}$, where j_{ki} is the total two-body angular momentum after coupling of j_i to the spin of the

$$(H) = \begin{pmatrix} E_{ki}^{(\ell_{ki},\frac{1}{2},j_{ki}=0)} + \frac{1}{4}E_{kj}^{(\ell_{kj},\frac{1}{2},j_{kj}=0)} + \frac{3}{4}E_{kj}^{(\ell_{kj},\frac{1}{2},j_{kj}=1)} & \frac{\sqrt{3}}{4}(E_{kj}^{(\ell_{kj},\frac{1}{2},j_{kj}=1)} - E_{kj}^{(\ell_{kj},\frac{1}{2},j_{kj}=0)}) \\ \frac{\sqrt{3}}{4}(E_{kj}^{(\ell_{kj},\frac{1}{2},j_{kj}=1)} - E_{kj}^{(\ell_{kj},\frac{1}{2},j_{kj}=0)}) & E_{ki}^{(\ell_{ki},\frac{1}{2},j_{ki}=1)} + \frac{3}{4}E_{kj}^{(\ell_{kj},\frac{1}{2},j_{kj}=0)} + \frac{1}{4}E_{kj}^{(\ell_{kj},\frac{1}{2},j_{kj}=1)} \end{pmatrix}. \quad (21)$$

core s_k. We denote the corresponding two-body eigenvalues by $E_{ki}^{(\ell_{ki},j_i,j_{ki})}$. The natural basis to describe the three-body system is then $\{|\,[s_k,(s_i,\ell_{ki})j_i]\,j_{ki},(\ell_{kj},s_j)j_j;J\rangle\}$, where J is the total three-body angular momentum. The two-body Hamiltonian H_{ki} with eigenvalues $E_{ki}^{(\ell_{ki},j_i,j_{ki})}$ is diagonal in this three-body basis. This is in contrast to the remaining two-body Hamiltonian H_{kj}.

We can calculate the matrix elements of the three-body Hamiltonian in this basis. With the expression

$$\begin{aligned} &|\,[s_k,(s_i,\ell_{ki})j_i]\,j_{ki},(\ell_{kj},s_j)j_j;J\rangle = \\ &\sum_{j_{kj}}(-1)^{j_{ki}+j_{kj}+j_i+j_j}\sqrt{2j_{ki}+1}\sqrt{2j_{kj}+1} \\ &\times\begin{Bmatrix} j_j & s_k & j_{kj} \\ j_i & J & j_{ki}\end{Bmatrix}|\,[s_k,(\ell_{kj},s_j)j_j]\,j_{kj},(s_i,\ell_{ki})j_i;J\rangle \end{aligned} \quad (19)$$

we obtain by recoupling that

$$\begin{aligned} \langle qj_{ki}|H|q'j'_{ki}\rangle &= \delta_{qq'}\delta_{j_{ki}j'_{ki}}E_{ki}^{(\ell_{ki},j_i,j_{ki})} \\ &+\delta_{qq'}(-1)^{j_{ki}-j'_{ki}}\sqrt{(2j_{ki}+1)(2j'_{ki}+1)} \\ &\times\sum_{j_{kj}}(2j_{kj}+1)E_{kj}^{(\ell_{kj},j_j,j_{kj})}\begin{Bmatrix} j_j & s_k & j_{kj} \\ j_i & J & j_{ki}\end{Bmatrix}\begin{Bmatrix} j_j & s_k & j_{kj} \\ j_i & J & j'_{ki}\end{Bmatrix}, \end{aligned} \quad (20)$$

where $q = \{\ell_{ki},\ell_{kj},j_i,j_j\}$. Therefore the three-body Hamiltonian is diagonal in blocks defined by the quantum numbers q.

As an example, we show the 2×2 block corresponding to a core and two light particles all three with spin 1/2. We further assume $j_i = j_j = 1/2$, and $J = 1/2$ confining j_{ki} and j_{kj} to the values 0 and 1. We note that eq. (20) depends on the two-body relative orbital angular momenta, ℓ_{ki} and ℓ_{kj}, only through the two-body energies. Then the corresponding block is given by

see eq. (21) *above*

This illustrates that even for the schematic case in fig. 1, where particles i and j do not interact with each other, the three-body Hamiltonian is not separable anymore. The three-body eigenvalues are then not given by the sum of the two-body eigenvalues. When particles i and j are identical and $\ell_{ki} = \ell_{kj} = \ell$, then $E_{ki}^{(\ell,\frac{1}{2},j_{ki}=0)} = E_{kj}^{(\ell,\frac{1}{2},j_{kj}=0)} = E^{(0)}$ and $E_{ki}^{(\ell,\frac{1}{2},j_{ki}=1)} = E_{kj}^{(\ell,\frac{1}{2},j_{kj}=1)} = E^{(1)}$, and the eigenvalues of the matrix (21) are $\frac{1}{2}E^{(0)} + \frac{3}{2}E^{(1)}$ and $\frac{3}{2}E^{(0)} + \frac{1}{2}E^{(1)}$. Only the first of these eigenvalues corresponds to an antisymmetric eigenfunction under exchange of particles i and j. It is precisely twice the average energy of the two two-body energies. Due to the Pauli principle, the two light fermions must occupy both the two possible two-body states with angular momentum $\frac{1}{2}$. Then the relevant energies are not the individual energies of the two two-body states, but their average value.

When none of the two-body interactions contains the spin-spin term we have that

$$E_{ki}^{(\ell_{ki},\frac{1}{2},j_{ki}=0)} = E_{ki}^{(\ell_{ki},\frac{1}{2},j_{ki}=1)} \equiv E_{ki}^{(\ell_{ki},\frac{1}{2})}, \quad (22)$$

$$E_{kj}^{(\ell_{kj},\frac{1}{2},j_{kj}=0)} = E_{kj}^{(\ell_{kj},\frac{1}{2},j_{kj}=1)} \equiv E_{kj}^{(\ell_{kj},\frac{1}{2})}, \quad (23)$$

and the Hamiltonian (21) is diagonal, with identical diagonal terms given by $E_{ki}^{(\ell_{ki},\frac{1}{2})} + E_{kj}^{(\ell_{kj},\frac{1}{2})}$, which is the result obtained in the previous section for spin-zero systems. When only one of the two-body interactions has a non-zero spin-spin term (*e.g.*, V_{ki}, eq. (22) is invalid and eq. (23) is valid) the Hamiltonian is diagonal in the basis $\{|\,[s_k,(s_i,\ell_{ki})j_i]\,j_{ki},(\ell_{kj},s_j)j_j;J\rangle\}$ with the energies $E_{ki}^{(\ell_{ki},\frac{1}{2},j_{ki}=0)} + E_{kj}^{(\ell_{kj},\frac{1}{2})}$ and $E_{ki}^{(\ell_{ki},\frac{1}{2},j_{ki}=1)} + E_{kj}^{(\ell_{kj},\frac{1}{2})}$. There are then two possible three-body states, that again are given by the sum of the two-body energies.

4 General properties

The results obtained in the previous section for the system in fig. 1 can be taken as a test for the numerical method used to compute three-body states. Taking then the schematic system as starting point we analyze the main properties of the three-body states, and how they evolve in the energy plane when different ingredients are added to the calculations.

4.1 Bound states and resonances

We maintain the schematic model where $V_{23} = 0$ and $m_1 = \infty$. We first assume that both V_{12} and V_{13} only act in relative p-waves producing resonances of complex energies E_{12} and E_{13}, respectively. The three-body computation then leads to the results shown in fig. 2 for a specific set of parameters. In the small panel, together with the discretized complex rotated three-body continuum states (plotted for three different scaling angles), there are two additional complex rotated branch cuts starting at each of the two-body resonance energies (crosses in the figure). These branch cuts correspond to two of the particles in a two-body resonant state and the third particle in the continuum. To keep the figure cleaner these cuts have not been plotted. Taking b as an arbitrary length unit, the three-body system has a resonance at the energy $2mb^2E/\hbar^2 = 0.097 - i0.040$,

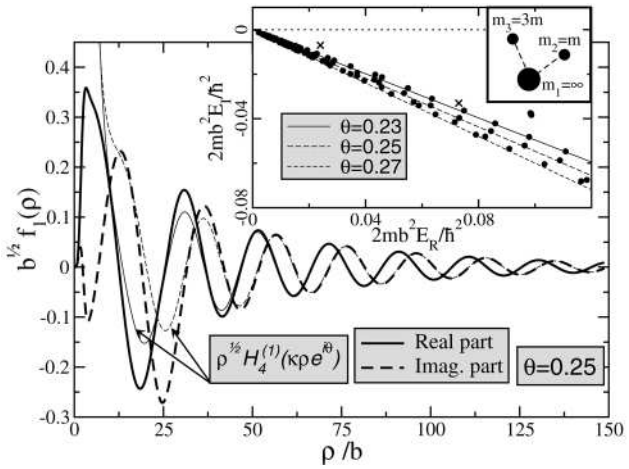

Fig. 2. Three-body resonance energy and radial wave function for $V_{23} = 0$ and two Gaussian p-wave interactions V_{12} and V_{13} with ranges $b_{12} = 1.5b$ and $b_{13} = b$. The strengths produce resonances at $2mb^2E_{12}/\hbar^2 = 0.073 - i0.033$, $2mb^2E_{13}/\hbar^2 = 0.024 - i0.007$. The masses are $m_1 = \infty$, $m_2 = m$, $m_3 = 3m$. Small graph: the solid, long-dashed and short-dashed lines connect the computed continuum spectra for rotation angles $\theta = 0.23$, 0.25, 0.27, respectively. The circle above these lines is a three-body resonance independent of θ. Big graph: the thick lines are the real (solid) and imaginary (dashed) parts of the lowest hyperradial adiabatic wave function of the three-body resonance when $\theta = 0.25$. The corresponding thin (solid, dashed) lines show the asymptotic behaviour.

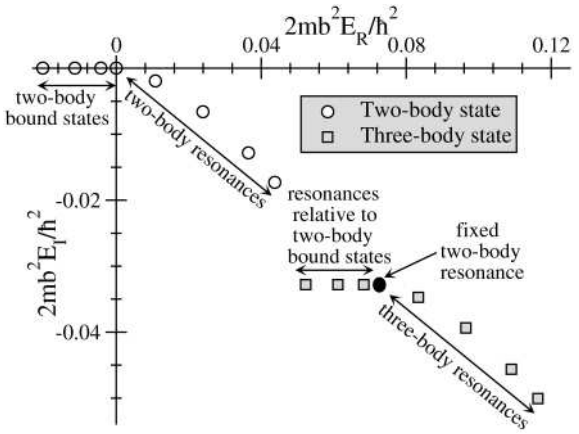

Fig. 3. Real (E_R) and imaginary (E_I) energy ($E = E_R + iE_I$) of the three-body states (squares) for a system with parameters as in fig. 2. The resulting energy is the sum of a fixed two-body resonance energy (black circle) and the energy of a varying two-body state (open circles). When this two-body state is bound the three-body state is the two-body resonance relative to the bound state.

clearly distinguishable from the continuum background and independent of the rotation angle. The computed energy is precisely at $E = E_{12} + E_{13}$, as found in sect. 3. This numerical result is then proving the efficiency of the numerical method. To illustrate that this indeed is a three-body resonance we also show the lowest radial wave function computed for a given rotation angle θ. Both the real and imaginary parts vanish asymptotically following the corresponding Hankel function $H^{(1)}_{K+2}$ as required for a pole of the S-matrix as seen from eq. (6).

When one of the two-body systems is bound and the other has a resonance the three-body state with energy equal to the sum of the two-body energies is simply a two-body resonance of one particle relative to the two-body bound state. This is illustrated in fig. 3, where one two-body resonance remains unchanged while the other two-body state is varied from resonance to bound state. When one two-body system is bound, and thus appearing on the negative real energy axis (open circles), the three-body energies (squares) appear at the same distances to the left of the fixed two-body resonance (black circle).

If the attractive interaction binding the two-body system decreases, at some point the two-body state enters through the origin into the fourth quadrant of the energy plane and becomes a two-body resonance. In parallel, the three-body energy (squares) approaches the two-body resonance energy (black circle) and continues through the two-body resonance in southeastern direction all the time following the addition rule.

4.2 Virtual states

The complex scaling method can be viewed as an analytic continuation into complex coordinates, such that resonances are "pulled out" of the continuum. Unfortunately the method fails when the pole corresponds to a virtual state, due to the necessary large rotation angle. Virtual states remain in the unphysical Riemann sheet, and numerical investigation of their effects is more difficult.

Let now the interactions V_{12} and V_{13} correspond to a virtual s-state and a p-resonance of energies E_{12} and E_{13}, respectively ($V_{23} = 0$, $m_1 = \infty$). Then, a 1^- three-body S-matrix pole should be present at $E = E_{12} + E_{13}$. To test this numerically we include an attractive s-wave interaction V_{23} which, combined with the other interactions, is sufficiently strong to reveal the existence of a 1^- three-body resonance. We show in fig. 4 how the complex energy of this resonance moves as the strength of V_{23} is varied. The strongest attraction (the point closest to the origin) corresponds to a virtual state in the 2-3 subsystem at an energy of about -0.004 in fig. 4. A very small additional attraction would bind the three-body system, which would be Borromean if the three-body system becomes bound before the 2-3 subsystem.

When the strength of V_{23} decreases the three-body resonance moves (closed circles) towards the energy E_{13} of the p-resonance. If we could track the three-body resonance for even weaker V_{23} we would for some non-zero value find that it precisely coincides with E_{13} (cross), reaching then the discontinuity cut of the Riemann sheet. For weaker V_{23} the three-body pole could move through this cut into any other Riemann sheet, but it is tempting to suggest that these states could be interpreted as two-body virtual s-states of particle 2 relative to the resonant state of particles 1 and 3. Thus such a three-body state is not a three-body resonance but a virtual state on the unphysical Riemann sheet, although it is not possible to

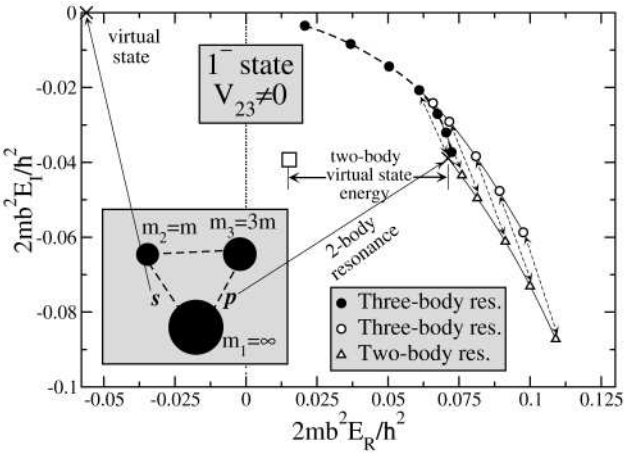

Fig. 4. Energies of the 1^- three-body states for a system with the same masses as in fig. 2. The p-wave and s-wave interactions, V_{13} and V_{12}, correspond to a resonance and a virtual state indicated by the crosses. The thick open square is the sum of the two two-body energies. Inclusion of a varying attractive s-wave interaction V_{23} leads to the three-body resonance energies given by the solid circles. For a fixed value of V_{23}, when the two-body p-resonance moves as shown by the open triangles, then the three-body resonances do it as given by the open circles.

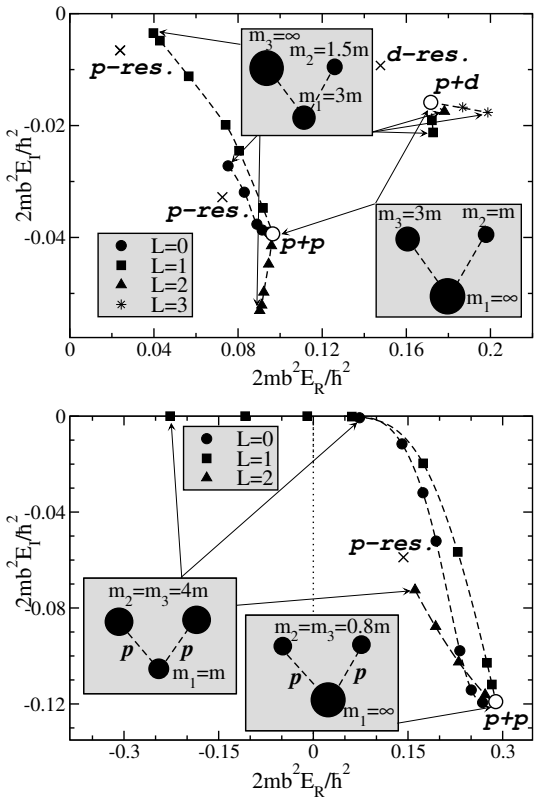

Fig. 5. Upper part: three-body resonances for a system with two-body reduced masses and resonance parameters as in fig. 2 ($p+p$ case). In the $p+d$ case the highest p-resonance has been substituted by a d-resonance with $2mb^2E_{12}/\hbar^2 = 0.145 - i0.009$. Lower part: three-body resonances for a system with $\mu_{12} = \mu_{13} = 0.8m$ and p-resonances at $E_{12} = E_{13}$ with $2mb^2E_{12}/\hbar^2 = 0.143 - i0.059$. The fixed two-body resonances are indicated by the crosses and the three-body resonances by a big open circle ($m_1 = \infty$), and solid circles ($L = 0$), squares ($L = 1$), triangles ($L = 2$), and asterisks ($L = 3$) for finite m_1 values.

see numerically how this energy (square) is reached when $V_{23} = 0$.

This can be better understood if the s-state is bound as illustrated in fig. 3. When the s-wave attraction is reduced until the bound-state energy is zero the three-body state moves in parallel towards the resonance energy. A continued decrease of the attraction turns the two-body bound state into a virtual s-state, and the two-body pole moves continuously from the physical to the unphysical Riemann sheet. In parallel, the three-body pole moves continuously through the p-resonance onto another Riemann sheet.

The connection between two and three-body resonances are very intimate even when all three masses and interactions are non-zero. This is emphasized in fig. 4 where V_{13} is varied for fixed V_{23}. Then the 1^- three-body resonances (open circles) follow precisely the motion of the two-body resonances (open triangles). The double arrows connect each two-body resonance with its corresponding three-body state. A variation of the two-body complex energy produces a similar energy change in the three-body state.

For completeness we also notice that virtual states in both subsystems lead to virtual three-body states with an energy following the sum rule and sitting in the negative energy axis of the unphysical Riemann sheet.

4.3 Finite mass and angular momentum coupling

In a less schematic model also m_1 has to be finite. Still often the three-body structure is mostly influenced by two two-body subsystems each dominated by one partial wave. Thus we relax the condition $m_1 = \infty$ but maintain the reduced masses μ_{12} and μ_{13} by adjusting m_2 and m_3. The two-body properties then remain unchanged for the same interactions V_{12} and V_{13}. The finite masses destroy the separability into two independent subsystems, and the eigenvalues of the three-body Hamiltonian are not any more given by the sum of the two-body eigenvalues. Also, a given combination of partial waves may couple to several total angular momenta with different energies.

When two partial p-waves both contribute, the total angular momentum and parity must be $L^\pi = 0^+$, 1^+, 2^+, and combining a p-wave and a d-wave we get $L^\pi = 1^-$, 2^-, 3^-. The corresponding threefold degeneracy is broken for finite m_1 as illustrated in the upper part of fig. 5. In general, for fixed structure of the system (fixed reduced masses, interactions, relative distances between particles ...), the three-body relative kinetic energy is smaller for finite mass of the core than for infinite mass, as seen by comparing $p_{ik}^2/2\mu_{ik} + p_{j,ik}^2/2\mu_{i,jk}$ in both cases. Thus the three-body resonances often tend to move towards the origin.

However, simultaneous conservation of angular momentum and center-of-mass might require a change of structure resulting in less total interaction energy than from the two resonances. Thus, the three-body resonance can move in all directions (fig. 5). As in the previous calculations, only the components corresponding to two-body resonances are included. The finite-mass effects are relatively small in all cases except for two p-waves coupled to $L^\pi = 1^+$. This can be understood by expressing the Faddeev component related to the 1-3 subsystem in the Jacobi coordinates of subsystem 1-2. For $L = 1$ a p-wave "rotates" fully into a p-wave. Then the p-wave attraction is fully exploited and the resulting three-body state has the lowest possible energy. When L and the two two-body angular momenta are equal there is a similar tendency, decreasing with L, to maximize the total attraction. Other components obtained by rotation are less important and uneven two-body angular momenta cannot exploit the attraction as efficiently, producing a much smaller change with m_1. In practice detailed quantum-mechanical computations are needed for each case to determine the size of the effects.

It is remarkable that the effects of the coupling and the center-of-mass motion can lower the energy sufficiently to produce a 1^+ three-body bound state (lower part of fig. 5). This is a Borromean system obtained by only two two-body interactions. When one resonance is replaced by a virtual state we have not numerically been able to find any three-body resonance produced entirely by finite-mass effects and without change of interactions.

5 Numerical illustrations

The origin of the resonances and bound states can be illustrated by different examples connecting the bare schematic model with well-known realistic nuclear structures. We first study two nucleons outside the spin-zero α-particle core, then we present detailed realistic computations for the same $A = 6$ systems, and finally we extend to the non-zero core-spin of the Borromean nucleus ^{17}Ne.

5.1 Core with zero spin

Let us consider a system made by an infinitely heavy core and two non-interacting spin-(1/2) particles. The core is assumed to be charged (with twice the proton charge) and the particle-core reduced mass is $0.8m$, where m is the nucleon mass. This system is very similar to an α-particle and two nucleons. The particle-core reduced mass is the same, and the center-of-mass effects are very small and not relevant for our present purpose [31].

Let us also consider a simple particle-core interaction given by a central short-range p-wave interaction producing a particle-core (uncharged) resonance at an energy of 0.74 MeV with a width of 0.60 MeV. When the light particle is assumed to have the proton charge, the same short-range interaction produces a core-particle resonance with energy and width of 1.60 MeV and 1.26 MeV, respectively.

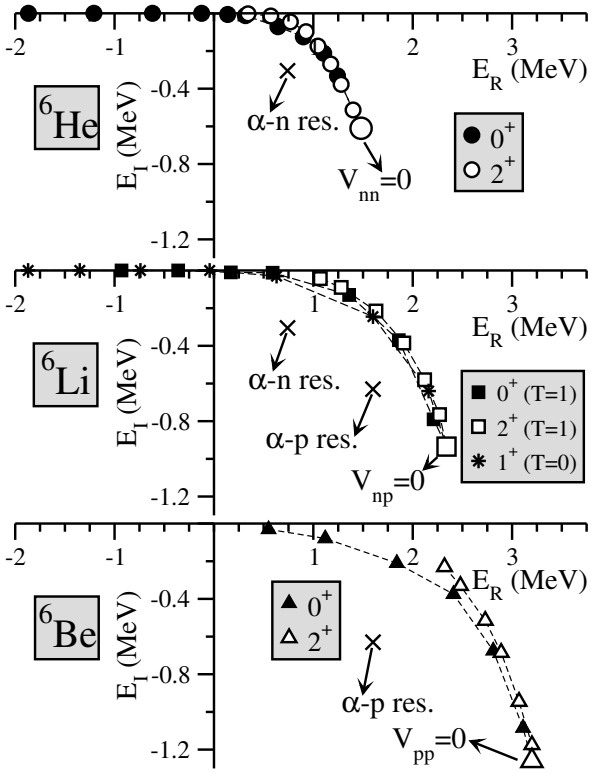

Fig. 6. Evolution of the three-body resonances for ^{6}He (circles), ^{6}Li (squares), and ^{6}Be (triangles), when the nucleon-nucleon interaction is progressively introduced. The big open symbols correspond to zero nucleon-nucleon interaction. The 0^+ and 2^+ resonances are shown by the closed and open symbols, respectively. The asterisks in the ^{6}Li case are the 1^+ resonance corresponding to the $T = 0$ channel in the neutron-proton interaction. The crosses show the alpha-nucleon resonance energies.

These values are consistent with the lowest p-resonances in ^{5}He and ^{5}Li, respectively [32].

In fig. 6, we show the results for one heavy and two light particles resembling the ^{6}He, ^{6}Li, and ^{6}Be systems. The upper, middle and lower parts correspond to both uncharged, one neutral and one with the proton charge, and both with the proton charge, respectively. When the nucleon-nucleon interaction is equal to zero, the three-body system must have a resonance at an energy equal to the sum of the two two-body resonance energies. This is again confirmed by calculations using the complex rotated adiabatic expansion method. We obtain the three-body resonances indicated by the big open circle, big open square, and big open triangle in the upper, central, and lower parts of fig. 6. They match precisely with the sum of the two-body energies each indicated by a cross.

The known spectrum for the schematic three-body system, determined completely by the internal two-body states, can be used as starting point to trace the connection with the "realistic" three-body system. This must be done by including the effects produced by i) an additional interaction between the two light particles, ii) quantum numbers conservation (like the angular momentum), and

iii) center-of-mass effects originating from the finite mass of the core.

Effects i) and ii) are closely connected. Once the interaction between the two light particles is included the three-body wave function, initially independent of the total angular momentum (eq. (12)), is now depending on L. This can be seen in the upper part of fig. 6, where we include the neutron-neutron interaction multiplied by a global factor varying from 0 to 1. Then the 0^+ and 2^+ states evolve as shown by the solid and open circles, respectively. When the full neutron-neutron interaction is included (last point on each curve), the system similar to ^{6}He has a bound Borromean 0^+ state (with a binding energy close to -1.9 MeV) and a very narrow 2^+ three-body resonance with energy 0.34 MeV.

For the system similar to ^{6}Li shown in the middle part of the figure one of the light particles has the charge of the proton. The neutron-proton interaction is again continuously switched on from zero to full strength. The 0^+ and 2^+ states ($T = 1$), analogous to those in the upper part, move as given by the closed and open squares, respectively. The final 0^+ state is still below the three-body threshold, with a binding energy of -1.0 MeV. The final 2^+ resonance has an energy of 1.1 MeV and a width of 0.1 MeV. The shift in energy compared to the states in the upper part is produced by the Coulomb repulsion between the core and the charged particle. Now the allowed $T = 0$ coupling gives rise to additional three-body states, *e.g.* the 1^+ state shown by the asterisks. When the three-body 1^+ state becomes bound the system is still Borromean. However, for some threshold strength the two light particles become bound, and the system is not Borromean anymore. When the full interaction is included the two light particles then form a deuteron nucleus, and the three-body 1^+ state becomes the ground state of the system, very similar to ^{6}Li, with a binding of about -5.5 MeV (outside the scale of the figure).

In the lower part of the figure we show results for two light particles each with the proton charge. As in the upper part only the $T = 1$ states are allowed, and since all the three two-body subsystems feel the Coulomb repulsion, the energies of the 0^+ states (closed triangles) and the 2^+ states (open triangles) are clearly larger than in the previous cases. In fact, when the full proton-proton interaction is included the 0^+ ground state is unbound, with resonance energy and width of 0.5 MeV and 0.2 MeV, respectively. For the 2^+ resonance the energy and width are 2.3 MeV and 0.5 MeV.

The effects produced by the finite mass of the core (center-of-mass effect), do not change the previous energies significantly (typically no more than 100 keV [31]). The spectra obtained for the "simplified" ^{6}He, ^{6}Li, and ^{6}Be nuclei (only a simple p-wave particle-core interaction has been used), indicate where to find the true states. This is seen in table 1, where the second column gives the computed energies. A comparison with the experimental results (last column) reveals that in all the three nuclei the main features of the spectrum are well reproduced. Therefore, starting from the schematic case where the three-body energy is given by the sum of the two-body energies and taking into account the main characteristics of the remaining two-body interaction, it is possible to estimate where the three-body states must be placed.

Table 1. Computed and experimental energies (in MeV) for ^{6}He, ^{6}Li, and ^{6}Be. The energies within brackets are (E_R, Γ_R), that give the resonance energy and its width. The computations correspond to the schematic system described in the text (second column), realistic calculations without inclusion of an effective three-body force (third column), and the same calculation when a three-body force is used (fourth column). The experimental values (last column) are taken from [32]. When not specified, the error bars are smaller than the last digit.

		Scheme	Real. (no 3-b)	Realistic	Exper.
^{6}He	0^+	-1.87	-0.04	-0.96	-0.97 ± 0.04
	2^+	(0.34,0.01)	(1.02,0.28)	(0.87,0.11)	(0.83,0.11)
	0^+	-0.93	(0.75,0.15)	-0.14	-0.14
^{6}Li	1^+	-5.60	-3.05	-3.73	-3.70
	2^+	(1.07,0.09)	(1.92,0.87)	(1.66,0.50)	(1.67,0.54)
^{6}Be	0^+	(0.55,0.16)	(2.05,0.58)	(1.37,0.11)	(1.37,0.09)
	2^+	(2.32,0.46)	(3.10,1.89)	(3.02,1.65)	(3.04,1.16)

As seen in the table, the computed energies are always lower than the experimental ones. This is because the nucleon-core interaction is without any spin-orbit term, and consequently the two possible p-resonances ($p_{1/2}$ and $p_{3/2}$) appear at the same energy. This is overbinding the system, since the $p_{1/2}$-resonance is known to be a few MeV higher [32], and a realistic calculation must include a repulsive term pushing up this resonance to the correct value. On top of this, other than p-waves should be included in the calculation. For s-waves the effect of the Pauli principle must be accounted for, since the $s_{1/2}$-shell is fully occupied in the α-core. This effectively amounts to a highly repulsive s-wave potential at short distances, also pushing the computed energies towards higher values. Furthermore, it is well known that three-body calculations using only realistic two-body interactions typically underbind the system. This can be cured by inclusion of an additional potential taking into account possible three-body effects to reproduce the experimental values.

Realistic detailed calculations using the (complex scaled) hyperspheric adiabatic expansion method concerning ^{6}He can be found in [33,34]. For completeness, we show in the next section the results obtained for ^{6}Li and ^{6}Be when similar calculations are performed.

5.2 Realistic calculations for ^{6}Li and ^{6}Be

In [33] the use of phase equivalent potentials is suggested as an efficient method to take into account the Pauli principle in three-body calculations. This method, together with the hyperspheric adiabatic expansion method, is used to compute the ground state of ^{11}Li and ^{6}He. Thus, for ^{6}He the alpha-neutron s-wave interaction is able to bind the neutron into a Pauli forbidden state. To exclude this

state we use a phase equivalent potential with exactly the same phase shifts for all energies, but with one less bound state. The p-wave interaction contains a central and a spin-orbit term, such that the $p_{3/2}$ and $p_{1/2}$ resonances in ^{5}He are placed at the experimental energy values [32]. The neutron-neutron interaction can also be found in [33].

The calculation using only the two-body interactions underbinds the three-body nucleus (third column in table 1), and an additional effective three-body force is needed to recover the experimental value (fourth column). In [34] the same method supplemented by complex scaling is used to compute the 2^+ resonance in ^{6}He. In the present work the calculation is slightly simplified by using a repulsive s-wave alpha-neutron interaction to take the Pauli principle into account. When the same phase equivalent potential as for the ground state is used, the computed 2^+ state in ^{6}He is also given in the third and fourth columns of table 1. As before, the calculation without a three-body force is underbinding the system by about 0.5 MeV, and an effective three-body force is again needed. In all the calculations the three-body force is assumed to be Gaussian with a range of 3 fm and the strength is adjusted to fit the experimental value. For bound states it is obviously possible to find a strength fitting precisely the experimental value. For resonances, this single parameter is fitting simultaneously the energy and the width of the resonance.

For ^{6}Li and ^{6}Be we perform exactly the same calculations but adding the corresponding Coulomb interaction for the two cases. The additional proton-core repulsion in ^{6}Li is pushing up the energies of the 0^+ and 2^+ states compared to the energies obtained for ^{6}He, and even more for ^{6}Be, where all the three two-body subsystems feel the Coulomb repulsion. The computed energies are again given in the third column of table 1 when only the two-body interactions are used. As before, an effective three-body interaction is needed to fit the experimental energies (fourth column). The 0^+ state in ^{6}Li is still below the two-nucleon separation energy threshold, although when the three-body interaction is suppressed the computed state appears to be unbound. Again, when the strength of the three-body force is used to match the experimental resonance energies, the widths are also well reproduced, except for the 2^+ state in ^{6}Be, where the width is significantly larger than the experimental value.

In addition to the 0^+ and 2^+ $T = 1$ states, in ^{6}Li it is also possible to have states with $T = 0$. These three-body states correspond to structures where the neutron and the proton form a deuteron (d) nucleus, suggesting a description of the nucleus as a $d+\alpha$ two-body system. Therefore, we have performed a three-body calculation, identical to the ones described above, but where the nucleon-nucleon interaction has been substituted by the $T = 0$ interaction used in [35]. This potential reproduces the experimental deuteron binding energy, root-mean-square radius, electric quadrupole moment, and provides a d-wave content of 5.6%. The correspondig computed energies for the 1^+ (ground) state are also given in table 1.

The three-body Thomas-Ehrman shifts [36] of these isobaric analog 0^+ and 2^+ states are then obtained from table 1, *i.e.* in MeV (1.40,1.17,1.05) and (1.83,1.80,1.65) for the realistic cases without and with three-body potential, respectively. The latter results coincide by definition with the experimental values. The decreasing tendency in the computed differences are due to the smaller energy and the larger radii which in turn leads to smaller effects of the Coulomb interaction. The underbinding is responsible for this discrepancy with measurements.

5.3 Core with non-zero spin

When the three particles have non-zero spins and spin-dependent two-body interactions, as in any realistic nuclear potential, then the three-body Hamiltonian is not even separable in the schematic model with an infinitely heavy core and two mutually non-interacting particles, see section 3.2. The Hamiltonian matrix is then organized in blocks with the matrix elements given by eq. (20).

An example is for ^{17}Ne, that is well described as a three-body system made by an ^{15}O core and two protons [37]. The core of the system has negative parity and spin 1/2. The two-body subsystem, ^{16}F (^{15}O+p), has four low-lying resonances, two of them (0^- and 1^-) arise from the coupling of a relative $s_{1/2}$-wave and the spin of the core, and other two (2^- and 3^-) result from the coupling between a $d_{5/2}$-wave and the spin of the core. The experimental energies and widths (E_R,Γ_R) of these two-body resonances are $(0.535, 0.040 \pm 0.020)$ MeV, $(0.728 \pm 0.006, 0.040)$ MeV, $(0.959 \pm 0.005, 0.040 \pm 0.030)$ MeV, and $(1.256 \pm 0.004, 0.004)$ MeV, respectively [38].

In [37] several proton-core interactions, all of them reproducing the experimental energies and widths, are given. These interactions contain spin-dependent operators, in particular the spin-splitting operator $\boldsymbol{s}_c \cdot \boldsymbol{j}_p$, where $\boldsymbol{s}_c$ is the spin of the core and $\boldsymbol{j}_p$ results from the coupling between the relative orbital angular momentum and the spin 1/2 of the proton. In the following calculations we shall use the s- and d-wave interactions corresponding to a Gaussian two-body potential with the parameters given in table 1 of [37], but where the spin-orbit strength has been modified to push away the $d_{3/2}$-resonances in ^{16}F, but keeping the two $d_{5/2}$-resonances at the right energy. In this way our slightly simplified ^{17}Ne is characterized exclusively by the 0^-, 1^-, 2^-, and 3^- resonances in ^{16}F, and we can perform for ^{17}Ne the same kind of analysis as in the previous cases.

Let us begin by performing calculations for the schematic model without any proton-proton interaction and for an infinitely heavy core. The effect of the finite mass of the core is clearly smaller than for ^{6}He, ^{6}Li, and ^{6}Be, and the core can safely be assumed to be infinitely heavy.

When both protons are in an s-wave relative to the core, only the 0^- and 1^- states in ^{16}F are obtained, and only the components with relative core-proton orbital angular momentum equal to zero are included in the calculation. In this case the total three-body angular momentum can only take the value $J = 1/2$ [37], and the block to be diagonalized is given in eq. (21). From the two

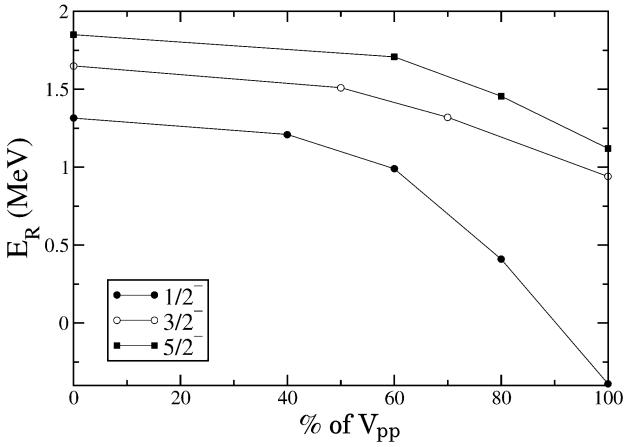

Fig. 7. ^{17}Ne energies for the $1/2^-$, $3/2^-$, and $5/2^-$ states as a function of the percentage of the proton-proton interaction included in the calculation.

possible eigenfunctions only one of them is antisymmetric under exchange of the two protons, and corresponds to the eigenvalue $(E^{(0^-)} + 3E^{(1^-)})/2$, that is twice the average energy of the two $s_{1/2}$-resonances. This gives rise to a $1/2^-$ energy of 1.32 MeV, that is recovered when the calculation using the complex scaled hyperspheric adiabatic expansion method is performed.

When the proton-proton interaction V_{pp} is progressively introduced, the contribution from the d-waves starts to be relevant, and the components with relative core-proton orbital angular momentum equal to 2 are also included. The energy of the $1/2^-$ state then changes as shown by the solid circles in fig. 7. Around 90% of the proton-proton interaction is already binding the three-body system, becoming then Borromean. The full proton-proton interaction gives a binding of about 0.40 MeV and a d-wave content of 37%. This binding is 0.3 MeV smaller than the one given in table 8 of [37]. This is due to the fact that in this calculation, in order to clean the structure of ^{17}Ne, we have artificially pushed up the $d_{3/2}$-resonances by using a large spin-orbit splitting. This is also reducing the d-wave content compared to the result in [37].

In ref. [37] we show how the $3/2^-$ state in ^{17}Ne is dominated by the sd-interferences between the components. To investigate this resonances both (0 and 2) core-proton relative orbital angular momenta are then needed and therefore included in the calculation. For the schematic ^{17}Ne model ($V_{pp} = 0$), one of the protons can be in one of the s-resonances in ^{16}F (0^- or 1^-), and the other can be in one of the $d_{5/2}$-resonances (2^- or 3^-). Assuming $J = 3/2$, the block in eq. (20) is already diagonal with only one non-zero energy equal to $E^{(1^-)} + E^{(2^-)}$. This energy of 1.65 MeV is recovered in the numerical calculation, which also reveals that the only non-vanishing components correspond to one proton in the s-wave 1^- resonance and the other in the d-wave 2^- resonance. The evolution of the energy when the proton-proton interaction is introduced is shown by the white circles in fig. 7, reaching a final value of 0.94 MeV. This value is also around 0.3 MeV less bound than the one given in table 8 of [37].

Finally, in the figure we also show the evolution of the lowest $5/2^-$ resonance in ^{17}Ne (solid squares) when V_{pp} is introduced. This state is also dominated by sd-interference components.

6 Qualitative considerations

Using the schematic case in which $V_{23} = 0$ as starting point, it is possible to trace the behaviour of the three-body resonances (figs. 2, 3, and 4) when the center-of-mass effects and the V_{23} interaction are included. Taking into account the main features of the V_{23} interaction, it is then possible to make crude estimates concerning different realistic systems.

For nuclear systems we take the mass unit m equal to the nucleon mass and a length unit equal to a typical range for the nuclear interaction ($b = 2$ fm). With this choice, the lowest p-resonance in the neutron-alpha interaction has dimensionless energy $2mb^2|E_R|/\hbar^2 \approx 0.15$. Therefore, in ^{6}He ($\alpha$+$n$+$n$), before including the neutron-neutron interaction, the three-body system must have a resonance with dimensionless energy of about 0.30. The neutron-neutron interaction has a low-lying virtual state at $2mb^2|E_R|/\hbar^2 \approx 0.02$, which is enough to bind the three-body state as evidenced by the bound state in ^{6}He at $2mb^2E_R/\hbar^2 \approx -0.19$.

For ^{11}Li (^{9}Li + n+n) the s-waves are pronounced and the lowest neutron-^{9}Li virtual s-state would after spin averaging appear at about 0.07 which, combined with the neutron-neutron interaction, is sufficient to bind the three-body system. Substituting ^{9}Li by a Λ-particle we arrive at an unstable system. With the Λ-nucleon s-wave scattering length of 2 fm obtained from hypertriton computations [35] the virtual s-state would be at around 1.7, too large to bind the Λ-neutron-neutron system.

We can continue to a more speculative system obtained by combining the recently discovered pentaquark resonance with a third particle like a meson. The pentaquark, θ^+, has a mass of 1540 MeV and decays mainly into a kaon K^+ and a neutron [39]. The energy above threshold is then around 107 MeV, that corresponds to a dimensionless energy of about 20. Thus, the neutron-neutron interaction, that was able to bind $\alpha + n + n$ and ^{9}Li + $n + n$, respectively with 0.15 and 0.07, but not $\Lambda + n + n$ with 1.7, cannot bind the $K^+ + n + n$ system. Thus a nucleon-kaon-meson cluster system would also exploit the intrinsic quark degrees of freedom and not resemble any three-body structure although additional binding would be picked up. In any case the narrow width of θ^+ strongly suggests that the resonance cannot have nucleon-kaon (two-particle) structure, but rather is a genuine five-quark system or perhaps a more exotic structure.

The semi-quantitative knowledge obtained with the schematic model can also be used for molecules due to the use of dimensionless parameters. For molecules we choose as typical scale units the mass of the ^{4}He atom and the range $b = 10$ Å. The ^{3}He + ^{4}He dimer has then

$2mb^2|E_R|/\hbar^2 \approx 0.75$ [40]. We can then expect that, except for center-of-mass effects, the trimers ^{3}He + ^{4}He + ^{4}He and ^{4}He + ^{3}He + ^{3}He should both have an unbound state with dimensionless energy of about 1.50 when the interaction between the two identical particles is neglected. However, including these interactions of dimensionless energies 0.02 for ^{4}He + ^{4}He and 5.2 for ^{3}He + ^{3}He, we arrive at trimers ^{3}He + ^{4}He + ^{4}He and ^{4}He + ^{3}He + ^{3}He, respectively bound and unbound as observed.

7 Summary and conclusions

The two-body interactions are assumed to determine completely the three-body structure including the continuum properties. Close to the threshold of binding, slightly above or below, the structure of the three-body system mostly depends on the two-body low-energy scattering properties. These properties are periodically repeated with increasing strengths of these attractive potentials corresponding to one or many bound states in each of the investigated channels. Therefore it is sufficient to study unbound or weakly bound two- and three-body systems.

The low-energy scattering properties are determined by the phase shifts and reflected in the poles of the S-matrix, *i.e.* by the resonances and virtual states. Thus, changing the two-body interactions simultaneously change the energies of both two- and three-body resonances. The relative changes of these energy observables are expected to be intuitively easier to understand than by using the connection via the two-body interaction strengths. The strategy is then to vary the two-body resonances and virtual states and study the changes of the corresponding quantities in the three-body system.

We employ the efficient and well-tested method of complex scaled hyperspherical adiabatic expansion. This method is first briefly sketched to define the notation. Then we define a schematic model with an infinitely heavy core and two mutually non-interacting particles. We prove mathematically for spin-zero particles that our formulation provides a pole in the three-body S-matrix if and only if the complex energy is equal to the sum of two complex energies each corresponding to poles of different two-body S-matrices for the two particle-core subsystems. The generalization to non-zero spins are formulated and shown to involve diagonalization of simple block-diagonal Hamiltonians.

The general properties are demonstrated numerically in schematic examples involving both resonances and virtual states. We then investigate the sizes and trends resulting from a finite core mass, non-zero interaction between the light particles and the coupling of different orbital angular momenta. We use dimensionless units to allow easy application on physics systems of different scales. Each of these effects can be substantial but the structure of the states can be uniquely traced back to the origin in the structure of the schematic model. Borromean systems can arise with only two interactions from center-of-mass effects and a favorable coupling of two angular momenta.

For further numerical illustration we use essentially realistic nuclear three-body systems, ^{6}He, ^{6}Li, and ^{6}Be, consisting of two nucleons and an α-particle to trace back their measured spectra to our bare schematic model. The effects of isospin symmetry and the mixing short-range and Coulomb interactions are then seen. For completeness, we also present unpublished and fully realistic calculations of ^{6}Li and ^{6}Be. The origin of the structure is still apparent, but to get accurate energies and wave functions we must include effects of spin-orbit couplings and the Pauli principle. Three-body Thomas-Ehrman shifts can then be studied for these isobaric analog states. Finally the effects of non-zero core spin is investigated for the Borromean nucleus ^{17}Ne consisting of ^{15}O and two protons.

In the last section we explain, and illustrate by examples, how to make qualitative estimates of the three-body energies and their structure from the two-body properties of the subsystems. First we test by known examples of Borromean halo nuclei, hypertriton, molecular helium clusters and the recently highlighted more speculative pentaquark.

In conclusion, we have demonstrated the strong correlation between two- and three-body resonances. The three-body energy and structure can be traced back to the properties of an infinitely heavy core and two non-interacting light particles. Substantial changes are often needed to arrive at accurate and realistic properties but the generic origin is apparent and revealing both structures and energies.

Appendix A. Useful integrals

The three-body S-matrix for the schematic model in eq. (17) is obtained through the definition in eq. (16) by inserting eq. (15) into eq. (12). Then the following integrals are needed:

$$\int_0^{\pi/2} \mathrm{d}\alpha (\sin\alpha)^{\ell_x+2}(\cos\alpha)^{\ell_y+2} P_n^{(\ell_x+\frac{1}{2},\ell_y+\frac{1}{2})}(\cos 2\alpha) \times h^{(1)}_{\ell_x}(k_x x) h^{(1)}_{\ell_y}(k_y y) = (-1)^n \pi (\sin\alpha_\kappa)^{\ell_x}(\cos\alpha_\kappa)^{\ell_y} \times P_n^{(\ell_x+\frac{1}{2},\ell_y+\frac{1}{2})}(\cos 2\alpha_\kappa) \frac{H^{(1)}_{K+2}(\kappa\rho)}{(\kappa\rho)^2}\,, \tag{A.1}$$

$$\int_0^{\pi/2} \mathrm{d}\alpha (\sin\alpha)^{\ell_x+2}(\cos\alpha)^{\ell_y+2} P_n^{(\ell_x+\frac{1}{2},\ell_y+\frac{1}{2})}(\cos 2\alpha) \times h^{(2)}_{\ell_x}(k_x x) h^{(2)}_{\ell_y}(k_y y) = 0\,, \tag{A.2}$$

$$\int_0^{\pi/2} \mathrm{d}\alpha (\sin\alpha)^{\ell_x+2}(\cos\alpha)^{\ell_y+2} P_n^{(\ell_x+\frac{1}{2},\ell_y+\frac{1}{2})}(\cos 2\alpha) \times h^{(1)}_{\ell_x}(k_x x) h^{(2)}_{\ell_y}(k_y y) = \int_0^{\pi/2} \mathrm{d}\alpha (\sin\alpha)^{\ell_x+2}(\cos\alpha)^{\ell_y+2} P_n^{(\ell_x+\frac{1}{2},\ell_y+\frac{1}{2})}(\cos 2\alpha) \times h^{(2)}_{\ell_x}(k_x x) h^{(1)}_{\ell_y}(k_y y) \stackrel{\rho\to\infty}{\longrightarrow} (-1)^n \pi (\sin\alpha_\kappa)^{\ell_x} \times (\cos\alpha_\kappa)^{\ell_y} P_n^{(\ell_x+\frac{1}{2},\ell_y+\frac{1}{2})}(\cos 2\alpha_\kappa) \frac{H^{(2)}_{K+2}(\kappa\rho)}{2(\kappa\rho)^2}\,. \tag{A.3}$$

References

1. M.C. Gutzwiller, Rev. Mod. Phys. **70**, 589 (1998).
2. G. Tanner, K. Richter, J.M. Rost, Rev. Mod. Phys. **72**, 497 (2000).
3. A. Kievsky, M. Viviani, S. Rosati, Nucl. Phys. A **577**, 511 (1994).
4. J.M. Richard, Phys. Rep. **212**, 1 (1992).
5. L.D. Faddeev, Sov. Phys. JETP **12**, 1014 (1961).
6. J. Carbonell, V.A. Karmanov, Phys. Rev. C **67**, 037001 (2003).
7. E. Nielsen, D.V. Fedorov, A.S. Jensen, E. Garrido, Phys. Rep. **347**, 373 (2001).
8. A.S. Jensen, K. Riisager, D.V. Fedorov, E. Garrido, Rev. Mod. Phys. **76**, 215 (2004).
9. W. Glöckle H. Witala, D. Hüber, H. Kamada, J. Golak, Phys. Rep. **274**, 107 (1996).
10. C.D. Lin, Phys. Rep. **257**, 1 (1995).
11. T.N. Rescigno, M. Baertschy, W.A. Isaacs, C.W. McCurdy, Science **286**, 2464 (1999).
12. E.O. Alt, S.B. Levin, S.L. Yakovlev, Phys. Rev. C **69**, 034002 (2004).
13. A. Delfino, T. Frederico, M.S. Hussein, L. Tomio, Phys. Rev. C **61**, 051301 (2000).
14. N.B. Shulgina, B.V. Danilin, L.V. Grigorenko, M.V. Zhukov, J.M. Bang, Phys. Rev. C **62**, 014312 (2000).
15. T. Myo, K. Kato, S. Aoyama, K. Ikeda, Phys. Rev. C **63**, 054313 (2001).
16. N. Michel, W. Nazarewicz, M. Ploszajczak, K. Bennaceur, Phys. Rev. Lett. **89**, 042502 (2002).
17. R.Id. Betan, R.J. Liotta, N. Sandulescu, T. Vertse, Phys. Rev. C **67**, 014322 (2003).
18. J. Jörres, M. Wiescher, F.-K. Thielemann, Phys. Rev. C **51**, 392 (1995).
19. E. Garrido, D.V. Fedorov, A.S. Jensen, Nucl. Phys. A **695**, 109 (2001).
20. E. Garrido, D.V. Fedorov, A.S. Jensen, H.O.U. Fynbo, Nucl. Phys. A **748**, 39 (2005).
21. E.A. Kolganova, A.K. Motovilov, Y.K. Ho, Nucl. Phys. A **684**, 623c (2001).
22. H. Witala, W. Glöckle, Phys. Rev. C **60**, 024002 (1999).
23. Z. Papp, J. Darai, C.-Y. Hu, Z.T. Hlousek, B. Kónya, S.L. Yakovlev, Phys. Rev. A **65**, 032725 (2002).
24. R. Lazauskas, J. Carbonell, Phys. Rev. C **70**, 044002 (2004).
25. Y.K. Ho, Phys. Rep. **99**, 1 (1983).
26. E. Garrido, D.V. Fedorov, A.S. Jensen, Phys. Rev. C. **68**, 014002 (2003).
27. A. Csótó, Phys. Rev. C **49**, 2244 (1994).
28. A. Csótó, Phys. Rev. C **49**, 3035 (1994).
29. S. Aoyama, S. Mukai, K. Kato, K. Ikeda, Prog. Theor. Phys. **93**, 99 (1995).
30. S. Aoyama, S. Mukai, K. Kato, K. Ikeda, Prog. Theor. Phys. **94**, 343 (1995).
31. E. Garrido, D.V. Fedorov, A.S. Jensen, Phys. Lett. B **600**, 208 (2004).
32. F. Ajzenberg-Selove, Nucl. Phys. A **490**, 1 (1988).
33. E. Garrido, D.V. Fedorov, A.S. Jensen, Nucl. Phys. A **650**, 247 (1999).
34. D.V. Fedorov, E. Garrido, A.S. Jensen, Few-Body Syst. **33**, 153 (2003).
35. A. Cobis, A.S. Jensen, D.V. Fedorov, J. Phys. G **23**, 401 (1997).
36. E. Garrido, D.V. Fedorov, A.S. Jensen, Phys. Rev. C **69**, 024002 (2004).
37. E. Garrido, D.V. Fedorov, A.S. Jensen, Nucl. Phys. A **733**, 85 (2004).
38. F. Ajzenberg-Selove, Nucl. Phys. A **460**, 1 (1986).
39. B. Schwarzschild, Phys. Today **56**, 19 (2003).
40. E. Nielsen, D.V. Fedorov, A.S. Jensen, J. Phys. B **31**, 40855 (1998).